Finding Ship Radars in SAR images: Localizing Radio Frequency Interference using Unsupervised Deep Learning.

Kristian Aa. Sørensen*†, Anders Kusk*‡, Henning Heiselberg *§, Peder Heiselberg *¶
*National Space Institute of Denmark
The Technical University of Denmark, Kgs. Lyngby, Denmark
†OrchID: 0000-0001-6443-1297
Email: kaaso@space.dtu.dk
‡OrchID: 0000-0001-7822-4758
§OrchID: 0000-0002-8847-634X
¶OrchID: 0000-0003-2229-2000

***Abstract*—Synthetic Aperture Radar (SAR) satellite images are used increasingly more to observe the maritime environment, but they sometimes experience image degradation caused by interfering signals from external radars. Few on-ground radars can cause Radio Frequency Interference (RFI) and the RFI information can therefore increase domain awareness. Localizing and characterizing RFI signals in the ocean might help classify otherwise overlooked ships as, *e.g.*, potential navy ships. In this study, we detect and localize RFI signals automatically in Sentinel-1 quick-look images. We localized several RFI signals mid-sea believed to be caused by ship-borne air-surveillance radars. This study shows that more information can be extracted from certain detected objects, such as ships, from SAR images.**

***Index Terms*—synthetic aperture radar (SAR), radio frequency interference (RFI), deep learning, convolutional autoencoder, anomaly classification and localization**

I. Introduction

New surveillance methods applicable for maritime domain awareness are essential for monitoring and controlling maritime traffic safety, smuggling, invasion of foreign navy, and more. Foreign navy, in particular, rarely broadcast, *e.g.*, identification or location information. Non-cooperative surveillance systems are therefore required.

Satellite-borne synthetic aperture radar (SAR) imaging sensors have all-weather, all-hours imaging capabilities, and can therefore be used to image, *e.g.*, non-cooperative ships [1]. However, emitted pulses from external active radars with similar center frequency as the SAR can cause interference in the SAR images. This is called Radio Frequency Interference (RFI) [2], [3] and is caused by, *e.g.*, wireless communication in the P- or L-band spectrum [4], by air-surveillance radars in the C-band spectrum, or by mutual RFI (MRFI) between two SAR satellites [5]–[7].

Reference. [8] analyzed the impact of RFI signals in SAR ship detection, and concluded that RFI signals pose a serious threat in automatic ship detection algorithms. More importantly, knowing that a detected vessel carries, *e.g.*, an air-surveillance radar provides valuable information to decision makers and gives important insights to the vessel characteristics, *i.e.*, tankers or fishing vessel do not carry air-surveillance radars but navy ships might.

The few published studies of RFI signals in SAR images focus on detecting images containing RFI signals [9], [10], or to remove the RFI signal using different mitigation techniques [11]–[14]. In particular, [9] implemented a global Sentinel-1 RFI contaminated probability map by exploiting the noise measurement of the rank echos in the level-0 Sentinel-1 data [15]. References. [10], [16] implemented CNNs as supervised binary classifiers in conjunction with local empirical thresholds and find images with RFI signals without localizing the signals. Most RFI deep learning algorithms in the literature are supervised, and are thus heavily dependent on the manually labeled training data or simulated data [10], [14], [16]–[19]. Reference. [20] detected and localized RFI signals using location specific threshold- and tolerance-values applied on a combination of the Sentinel-1 VV and VH polarizations by assuming that a RFI was present in each analyzed image.

Localizing RFI signals in SAR images could therefore enhance maritime domain awareness by increasing the amount of detected non-cooperative ships and more importantly by providing valuable information on the detected vessel.

In this study, we present an unsupervised RFI localization method using deep learning. RFI signals mid-ocean can be caused by, *e.g.*, air-surveillance radars on-board ships. Localizing the RFI signal can therefore be valuable in increasing maritime domain awareness.

II. Method and materials

Anomalies were detected in Sentinel-1 quick-look images with an unsupervised convolutional autoencoder whereafter the anomalies were localized and classified as RFI signals.

Funding agency: The Danish Ministry of Defence Acquisition and Logistics Organisation (DALO)

A. RFI in Sentinel-1

A RFI signal is an external contribution, P_I, caused by an external radar with a similar center frequency, emitting a signal towards the receiving SAR antenna. The total received signal, P_r is then given by

$$P_r = P_{rs} + P_N + P_I, \tag{1}$$

where P_N is the noise contributions and P_{rs} is the contribution of the received signal from the transmitted SAR signal.

RFI signals originating from an external radar, P_I, using a different pulse modulation that the Sentinel-1 satellite will not be compressed in the range direction of the Sentinel-1 image and may even be extended beyond their original length, dependent on the RFI pulse modulation. A RFI will therefore, for the Interferometric Width (IW) operational mode extent for one or more swaths in the range direction. In the azimuth direction, an RFI pulse from a single echo is a delta function, and will thus be smeared over all focused image lines to which the RFI-affected pulse contributes.

B. Convolutional Autoencoders (CAE)

In an autoencoder, a model is trained to reconstruct the original input by parameterizing the input, $\boldsymbol{x}$, into a latent space, $\boldsymbol{z}$. For a good $\boldsymbol{z}$, the autoencoder learns how to reconstruct a noise-free sample and can therefore be used to automatically and unsupervised find anomalies by comparing a single input $\boldsymbol{x}_m$ with the reconstructed $\hat{\boldsymbol{x}}_m$, *i.e.*, a sample is anomalous when $\boldsymbol{x}_m \not\approx \hat{\boldsymbol{x}}_m$. An autoencoder finds all anomalies in the data, but does not classify the type of anomaly as, *e.g.*, an RFI signal.

An encoder maps an input, $\boldsymbol{x}_m$ into a smaller latent space, $\boldsymbol{z}_m$, as

$$g_\phi : \boldsymbol{x}_m \in \mathbb{R}^{d(\boldsymbol{x})} \rightarrow \boldsymbol{z}_m \in \mathbb{R}^{d(\boldsymbol{z})}, \tag{2}$$

where the latent space dimension is smaller than the input dimension, *i.e.*, $d(\boldsymbol{z}) \ll d(\boldsymbol{x})$. A decoder then makes a reconstruction, $\hat{\boldsymbol{x}}_m$, of the original input

$$q_\theta : \boldsymbol{z}_m \in \mathbb{R}^{d(\boldsymbol{z})} \rightarrow \hat{\boldsymbol{x}}_m \in \mathbb{R}^{d(\boldsymbol{x})}. \tag{3}$$

The objective of a convolutional autoencoder (CAE) is to reconstruct an input array using convolutional operations. For $d(\boldsymbol{z}) \approx d(\boldsymbol{x})$, a CAE likely overfit the training data and make a perfect reconstruction of the training images. Conversely, a too small $d(\boldsymbol{z})$ does not allow for the decoder to reconstruct an image.

C. Dataset

334 ascending Sentinel-1 quick-look images were acquired from a region near Japan using Alaskan Satellite Facility (ASF) DAAC and processed by ESA. The images were divided into a training-set consisting of 219 RFI-free images and a testing-set consisting of 115 either RFI-affected and RFI-free images. The CAE could not reconstruct the large-scale spatial structure of the RFI and the quick-look resolution were therefore sufficient for both RFI detection and localization.

All images were normalized with the min-max normalization using the values from the training data and center-cropped to the same size of 340x500x2, where the last channel corresponds to the VV and VH polarizations. Figure 1 shows a subset of the testing data with the VV polarization (left) and VH polarization (right). Some RFI signals are very visible (top), while some are not (bottom). We see that the RFI signals are elongated in range direction at the length of a swath, and that the azimuth extent are on the order of 3-5 km, as explained in Section II-A.

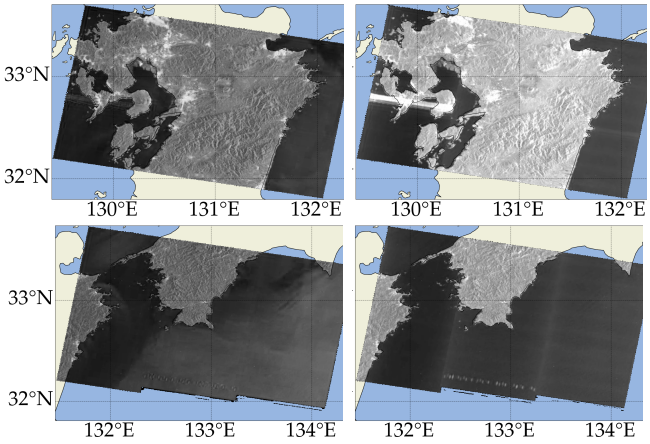

Fig. 1. Subset of the test data with (top): a very visible RFI signal and (bottom): a less visible RFI. (left): VV polarization, and (right): VH polarization.

D. CAE reconstruction

The CAE model was implemented using Tensorflow 2.10 and is described in Figure 2. Each layer was followed by a batch normalization and the first 2 layers of the encoder were likewise followed by a max-pooling layer. The loss function for the reconstruction error, $\mathcal{L}$, was defined using the structural similarity measure (SSIM) by maximizing the perceptual similarity between $\boldsymbol{x}$ and $\hat{\boldsymbol{x}}$, applied on each polarization and averaged [21], [22]:

$$\mathcal{L}(\boldsymbol{x}, \hat{\boldsymbol{x}}) = 1 - \left(\frac{(2\boldsymbol{x}\hat{\boldsymbol{x}} + C_1)(2s_{\boldsymbol{x}\boldsymbol{x}} + C_2)}{(\boldsymbol{x}^2 + \hat{\boldsymbol{x}}^2 + C_1) + (s_{\boldsymbol{x}}^2 + s_{\hat{\boldsymbol{x}}}^2 + C_2)} \right), \tag{4}$$

where C_1 and C_2 are added to avoid numerical instability. Consequently, $\hat{\boldsymbol{x}} \approx \boldsymbol{x}$ for $\mathcal{L}(\boldsymbol{x}, \hat{\boldsymbol{x}}) \rightarrow 0$ and $\hat{\boldsymbol{x}} \not\approx \boldsymbol{x}$ for $\mathcal{L}(\boldsymbol{x}, \hat{\boldsymbol{x}}) \rightarrow 1$. A batch size of 6 was used with a reducing learning rate with the Adam optimizer.

1) RFI classification and localization: Only large scale anomalies were found where $\hat{\boldsymbol{x}} \not\approx \boldsymbol{x}$ and RFI signals were classified by exploiting the elongation of the signals in range direction.

A heat map, $\mathbf{H}_m$ for image $\boldsymbol{x}_m$, was made using a SSIM running kernel of size 10x30, showing regions with large reconstruction errors in image $\boldsymbol{x}_m$. Large pixel-wise anomalies, $\mathbf{A}_m^{j,k} = |\boldsymbol{x}_m^{j,k} - \hat{\boldsymbol{x}}_m^{j,k}|$ where then found in regions with large reconstruction errors, *i.e.*, where $\mathbf{H}_m^{j,k} > 0.15$ and thereby removing small, insignificant local reconstruction

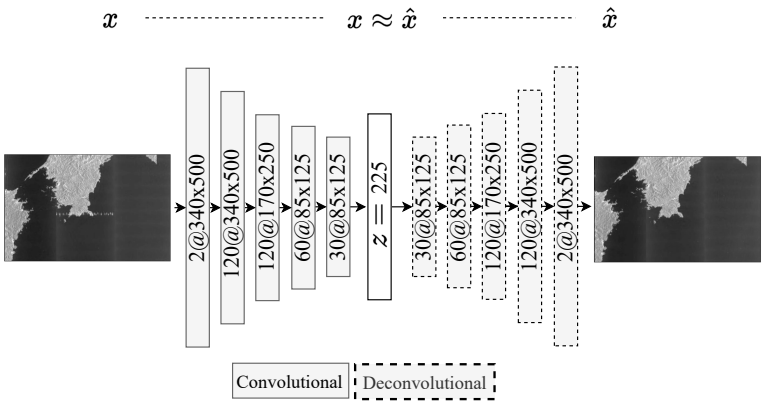

Fig. 2. Diagram of the Convolutional Autoencoder (CAE) reconstruction model.

errors. Elongated anomalies were found in a score-map, $\mathbf{S}_i$, calculated from the sum of errors in $\mathbf{A}_i$ in image patches of size 30x163, effectively divided column-wise into three swaths similar to the swaths of the Sentinel-1 satellites and row-wise to determine approximately which burst the RFI was located in. RFI anomalies were defined where $\mathbf{S}_m^{j,k} > 25$. Such that if the sum of a single "burst" in a single "swath" had a reconstruction error larger than 25, it is defined as a RFI anomaly, independent on both geographical region or location.

III. Results

The CAE was trained on a Nvidia Tesla v100 32 GB GPU and used to reconstruct the original SAR images whereafter the RFI anomalies were found by analyzing the elongated reconstruction errors.

A. CAE reconstruction

Figure 3 illustrates the total reconstruction error of all the training and testing images, inferred from the model with the lowest validation loss. The testing reconstruction errors were higher due to the RFI-affected SAR images, and were not caused by an overfitting of the training images. However, since the CAE was unsupervised it could not, by the reconstruction error alone, be verified if the high reconstruction errors were due to RFI signals or from other anomalies.

In Figure 4 we see a RFI affected image with (top left) the VH polarization, (top right) the VV polarization, and (bottom) the corresponding reconstructions. For the VV polarization, we see how the ocean state was somewhat reconstructed, with high and low intensity regions preserved, see, *e.g.*, top left and bottom right of the VV images. Likewise, for the VH polarization, we see that the RFI signal was not reconstructed. The CAE thus reconstructed the normality of the scene, but not the RFI signal.

B. RFI localization

Figure 5 illustrates the localized RFI signals in four images from the same region. Our method detected RFI signals at

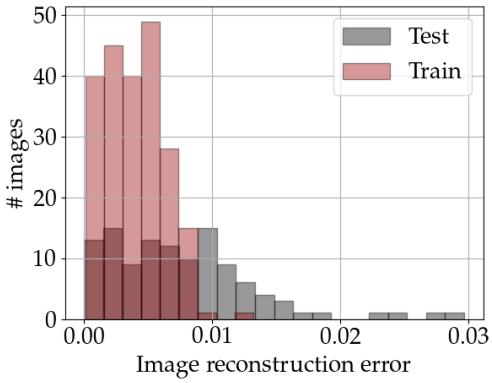

Fig. 3. Training and testing reconstruction error. A high reconstruction error corresponds to images not well reconstructed, possibly stemming from a RFI signal.

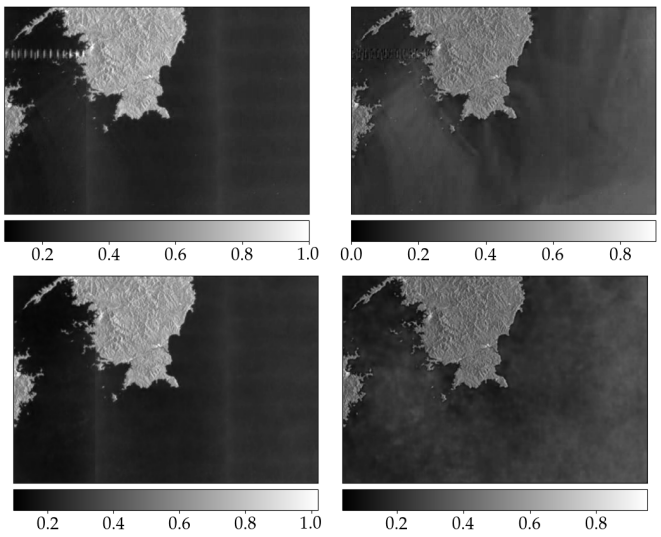

Fig. 4. (left): VH polarizations, (right): VV polarizations with (top): the original inputs and (bottom): the reconstructions.

varying locations at sea, *i.e.*, none of the RFI signals were geographically stationary in time. Moreover, the RFI signals in Figure 5 were only visible in the VH polarizations, as in the bottom of Figure 1.

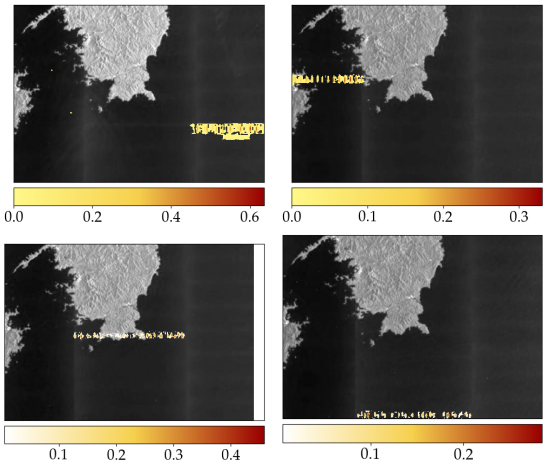

Fig. 5. Localized RFI signals in different VH polarized SAR images.

IV. Discussion

In this paper, we localize RFI signals in Sentinel-1 GRD quick-look images using an unsupervised CAE and a global RFI-optimized localization thresholds. The CAE reconstructs the RFI-free regions in the images while the RFI-affected regions have large reconstruction errors. Using the reconstruction errors, we find all anomalies in the images whereafter we classify them as RFI anomalies using a global threshold applied to sub-regions corresponding to specific bursts in the images.

Prior work has found RFI signal in Sentinel-1 level-0 data. However this is highly computational. Conversely, finding RFI in, *e.g.*, quick-look images reduces the needed computational power. Reference. [20] localized RFI signals in few images using a manual threshold-based method. However, static threshold methods are not generalizable and thresholds must be found empirically for every region and cannot be used for images under varying geographical or environmental conditions. Our method is unsupervised and employs a global threshold and can therefore be applied on other regions, assuming a RFI-free training-set is available. There is no need for local, manually derived thresholds. Moreover, instead of creating a training-set of SAR images containing RFI signals, we use a training-set without RFI signals. Furthermore, our method can both determine if a RFI signal is present and localize the RFI signal in the SAR image. The method can therefore be used to monitor both the activity and movement of RFI signals.

The RFI signals are caused by external radars, and by localizing them we gain insights into the location of the external radars. In the ocean it is highly likely that the RFI signals are caused by either air-surveillance radars or C-band SAR MRFI. The MRFI locations can be inferred using the known orbits of the SAR satellites. Even if the orbits are unknown, MRFI often have periodical structures in the entire images [5]. Furthermore, most of the localized RFI signals are only present in the VH polarization thereby insinuating that the signals were emitted directly to the satellite by a horizontally polarized radar. Historically, both weather radars and air-surveillance radars use horizontally polarized radars.

Occasionally, the localized RFI signals show periodical structures in the range direction. This might be caused by varying pulse repetition frequencies of the external radars within the sensing time of the SAR images, often seen for air-surveillance radars trying to avoid the blind-speed problem. Some of the localized RFI signals are therefore believed to originate from ship-based air-surveillance radars. The locations of the RFI signals might therefore providing valuable information on where possible ships using air-surveillance radars are located.

Acknowledgment

The authors would like to thank the Danish Defense and the Royal Danish Arctic Command for support and for sharing challenges, and the European Space Agency for providing the SAR scenes.

References

[1] P. Heiselberg, K. Aa. Sørensen, H. Heiselberg, O. B. Andersen, "SAR Ship & Iceberg Discrimination in Arctic Conditions Using Deep Learning," in Remote Sensing, vol. 14, 2022.

[2] P. De Matthaeis, R. Oliva, Y. Soldo, S. Cruz-Pol, "Spectrum Management and Its Importance for Microwave Remote Sensing [Technical Committees]" in IEEE Geoscience and Remote Sensing Magazine, vol 6, 2018.

[3] M. Tao, J. Su, Y. Huang, L. Wang. "Mitigation of Radio Frequency Interference in Synthetic Aperture Radar Data: Current Status and Future Trends," in Remote Sensing, vol. 11, 2019

[4] R. Natsuaki, T. Motohka, T. Suzuki, "Polarimetric characteristics of temporarily coherent RFI in alos-2 palsar-2," in 2017 IEEE International Geoscience and Remote Sensing Symposium (IGARSS), pp. 3155-3158, 2017.

[5] N. Li, Z. Lv, Z. Guo, "Observation and Mitigation of Mutual RFI Between SAR Satellites: A Case Study Between Chinese GaoFen-3 and European Sentinel-1A," in IEEE Transactions on Geoscience and Remote Sensing, vol. 60, pp. 1-19, 2022.

[6] P. Meadows, G. Hajduch, N. Miranda, "Sentinel-1 Long Duration Mutual Interference," December 2018.

[7] G. Hajduch, P. Meadows, N. Miranda, "Sentinel-1 Radarsat-2 Mutual Interference," November 2017.

[8] P. Shao, X. Lu, P. Huang, W. Xu, Y. Dong, "Impact Analysis of Radio Frequency Interference on SAR Image Ship Detection Based on Deep Learning," in International Geoscience and Remote Sensing Symposium (IGARSS), pp. 2447-2450, 2020.

[9] A. Monti-Guarnieri, D. Giudici, A. Recchia, "Identification of C-Band Radio Frequency Interferences from Sentinel-1 Data," in Remote Sensing, vol. 9, 2017.

[10] P. Artiemjew, A. Chojka, J. Rapiński, "Deep Learning for RFI Artifact Recognition in Sentinel-1 Data," in Remote Sensing, vol. 13, 2021.

[11] A. Recchia, D. Giudici, R. Piantanida, N. Franceschi, A. Monti-Guarnieri, N. Miranda, "On the Effective Usage of Sentinel-1 Noise Pulses for Denoising and RFI Identification," in EUSAR 2018; 12th European Conference on Synthetic Aperture Radar, pp. 1-5, 2018.

[12] W. Fan, F. Zhou, M. Tao, X. Bai, P. Rong, S. Yang, T. Tian, "Interference Mitigation for Synthetic Aperture Radar Based on Deep Residual Network," in Remote Sensing, vol. 14, 2019.

[13] P. Parasher, K. M. Aggarwal, V. M. Ramanujam, "RFI detection and mitigation in SAR data," in 2019 URSI Asia-Pacific Radio Science Conference (AP-RASC), pp. 1-4, March 2019.

[14] J. Yu, J. Li, B. Sun, J. Chen, C. Li, “Multiclass Radio Frequency Interference Detection and Suppression for SAR Based on the Single Shot MultiBox Detector,” in Sensors, vol. 18, 2018.
[15] G. Hajduch, N. Franceschi, M. Pinheiro, A. Valentino “SAR-MPC Sentinel-1: Using the RFI annotations,” February 2022.
[16] A. Chojka, P. Artiemjew, J. Rapiński, “RFI Artefacts Detection in Sentinel-1 Level-1 SLC Data Based On Image Processing Techniques,” in Sensors, vol. 20, 2022.
[17] J. Yu, J. Li, S. Bing, J. Yumin, “Barrage jamming detection and classification based on convolutional neural network for synthetic aperture radar,” in International Geoscience and Remote Sensing Symposium (IGARSS), pp. 4583-4586, July 2018.
[18] W. Fan, F. Zhou, M. Tao, X. Bai, P. Rong, S. Yang, “Interference Mitigation for Synthetic Aperture Radar Based on Deep Residual Network,” in Remote Sensing, vol. 11, 2019.
[19] W. Fan, F. Zhou, P. Rong, X. Yao, “Interference Mitigation for Synthetic Aperture Radar Using Deep Learning,” in 6th Asia-Pacific Conference on Synthetic Aperture Radar, APSAR, 2019.
[20] X. Leng, K. Ji, G. Kuang, “Radio Frequency Interference Detection and Localization in Sentinel-1 Images,” in IEEE Transactions on Geoscience and Remote Sensing, vol. 59, pp. 9270-9281, November 2021.
[21] Z. Wang, E. P. Simoncelli, A. C. Bovik, “Multiscale structural similarity for image quality assessment,” in The Thirty-Seventh Asilomar Conference on Signals, Systems & Computers, vol. 2, pp. 1398-1402, November 2003.
[22] Z. Wang, A. C. Bovik, H. R. Sheikh, E. P. Simoncelli, ”Image quality assessment: from error visibility to structural similarity,” in IEEE Transactions on Image Processing, vol. 13, pp. 600-612, April 2004, doi: 10.1109/TIP.2003.819861.
[23] T. O’Malley, E. Bursztein, J. Long, F. Chollet, J. Haifeng, L. Invernizzi et al., ”KerasTuner,” online at https://github.com/keras-team/keras-tuner, 2019.